Finding spin-glass ground states using quantum walks

Adam Callison[1], Nicholas Chancellor[2], Florian Mintert[1] and Viv Kendon[2]

[1] Blackett Laboratory, Imperial College London, London SW7 2BW, UK
[2] Department of Physics, Durham University, South Road, Durham, DH1 3LE, UK

E-mail: viv.kendon@durham.ac.uk, a.callison16@ic.ac.uk

Abstract. Quantum computation using continuous-time evolution under a natural hardware Hamiltonian is a promising near- and mid-term direction toward powerful quantum computing hardware. We investigate the performance of continuous-time quantum walks as a tool for finding spin glass ground states, a problem that serves as a useful model for realistic optimization problems. By performing detailed numerics, we uncover significant ways in which solving spin glass problems differs from applying quantum walks to the search problem. Importantly, unlike for the search problem, parameters such as the hopping rate of the quantum walk do not need to be set precisely for the spin glass ground state problem. Heuristic values of the hopping rate determined from the energy scales in the problem Hamiltonian are sufficient for obtaining a better than square-root scaling. This makes it practical to use quantum walks for solving such problems, and opens the door for a range of applications on suitable quantum hardware.

Contents

1. Introduction

Optimization problems need to be solved in a broad range of areas. This is often computationally intensive, so the prospect of quantum enhanced solution methods is an important research direction for practical quantum computing. A natural way to tackle optimisation in a quantum setting is to use a device which realises an Ising Hamiltonian with a transverse field. The optmisation problem is encoded into the Ising Hamiltonian $\hat{H}_I$

$$\hat{H}_I = -\sum_{(j\neq k)=0}^{n-1} J_{jk}\hat{Z}_j\hat{Z}_k - \sum_{j=0}^{n-1} h_j\hat{Z}_j, \tag{1}$$

on n qubits, such that the solution corresponds to the ground state of $\hat{H}_I$. The (real) values of the coupling strengths J_{jk} and fields h_j are determined by the optimisation problem, and $\hat{Z}_j$ is the operator on the full Hilbert space that applies the single qubit Pauli-Z operator $\hat{Z}$ to the jth qubit,

$$\hat{Z}_j = \left(\bigotimes_{r=1}^{j-1}\hat{\mathbb{1}}_2\right)\otimes\hat{Z}\otimes\left(\bigotimes_{r=j+1}^{n}\hat{\mathbb{1}}_2\right), \tag{2}$$

where $\hat{\mathbb{1}}_2$ is the identity operator on a single qubit. The transverse field term $\hat{H}_T$

$$\hat{H}_T = -\Gamma\sum_{j=0}^{n}\hat{X}_j, \tag{3}$$

drives transitions between states, where Γ is a real-valued transverse field strength, and $\hat{X}_j$ is the operator on the full Hilbert space that applies the single qubit Pauli-X operator to the jth qubit, defined by analogy with $\hat{Z}_j$ in (2). The computation is carried out by the dynamics induced by the, in general time-dependent, Hamiltonian

$$\hat{H}_{\mathrm{TIM}}(t) = A(t)\hat{H}_I + B(t)\hat{H}_T, \tag{4}$$

where t is time and $A(t)$, $B(t)$ are real-valued control functions. To obtain a candidate solution to the optimisation problem, the qubit register is measured after a time t_f. For some problems, sampling from the distribution of low energy states provides the required solution – this can be done by repeating the computation, which will in general not produce the lowest energy state with certainty.

The Ising Hamiltonian is chosen for encoding problems for two reasons. First, it is proven to be universal for all classical spin problems (De las Cuevas and Cubitt, 2016). There are efficient methods for mapping NP-Hard optimization problems to the Ising model (Lucas, 2014; Choi, 2010), providing a practical route to quantum algorithms. Promising results have been presented for a wide range of applications, such as mathematics (Bian et al., 2013; Li et al., 2017), computer science (Chancellor et al., 2016), computational biology (Perdomo-Ortiz et al., 2012), finance (Marzec, 2016), and aerospace (Coxson et al., 2014). Secondly, the Ising Hamiltonian can be implemented in many different physical systems. The quantum Ising Hamiltonian is the basic interaction Hamiltonian in the D-Wave Systems Inc. programmable superconducting devices (D-Wave, 1999–; Boixo et al., 2013; Johnson et al., 2011). Implementations in other promising architectures include Rydberg systems (Bernien et al., 2017); the Ising Hamiltonian is also the basic tool for other specialised optimization hardware, such as coherent Ising machines (Inagaki et al., 2016; McMahon et al., 2016). Ising Hamiltonian-based optimisation can be implemented in digital quantum architectures by using the quantum approximate optimisation algorithm (QAOA) (Farhi et al., 2014a,b; Marsh and Wang, 2019) or quantum alternating operator ansatz (Hadfield et al., 2019). These algorithms can thus be exploited in the many current efforts to build circuit model quantum computers.

There are several known methods for driving the quantum system from an initial state into the ground state of a problem Hamiltonian, corresponding to different choices for the control functions $A(t)$ and $B(t)$ in (4). Adiabatic quantum computing (Farhi et al., 2000, 2001) keeps the quantum system in the ground state throughout the evolution as the initial Hamiltonian is slowly changed into the problem Hamiltonian. Quantum annealing (Finnila et al., 1994; Kadowaki and Nishimori, 1998) takes advantage of open quantum systems effects to cool the system. Quantum walks evolve the system under the time-independent transverse Ising Hamiltonian for a suitable time before measurement of the final state. The ground state will in general be found with probability less than one; hence, repeats will be required to amplify the success probability. Computation by continuous-time quantum walk and adiabatic quantum computing are end points of a family of continuous-time protocols that use the same Hamiltonian terms but are applied with different time dependent modulation (Morley et al., 2019).

Quantum walks can solve the search problem (Childs and Goldstone, 2004), achieving the same quadratic $O(N^{1/2})$ quantum speed up as is obtained by Grover's algorithm (Grover, 1996). For particular graphs, quantum walks can solve problems exponentially faster (e.g., Childs et al., 2003), and quantum walks are now widely used as subroutines in more complex quantum algorithms. However, in the continuous-

time setting, the application of quantum walks to optimisation problems has not yet been studied in detail, although there is increasing interest in quenches (Amin et al., 2018) or pauses (Marshall et al., 2018; Passarelli et al., 2019) in quantum annealing, which effectively run a quantum walk during part of the computation. Given that quantum walks provide the best performance for searching when several types of realistic imperfections are considered (Morley et al., 2019), it is important to understand how they perform for a wider range of problems. In this work, we apply the continuous-time quantum walk to a problem that is similar to real optimisation problems to tackle the question of if, and how, a quantum walk can be useful for practical quantum optimisation.

Finding the ground state of a frustrated Sherrington-Kirkpatrick spin glass (Sherrington and Kirkpatrick, 1975) is known to be not only NP-Hard, but also *uniformly*-hard, due to its finite-temperature spin glass transition. As has been shown for a random problem type used in early benchmarks of quantum annealing hardware (Katzgraber et al., 2014), uniform hardness is crucial: without this property, *randomly* generated instances of NP-Hard problems are not necessarily hard to solve (Beier and Vöcking, 2004; Krivelevich and Vilenchik, 2006; Lucas, 2014).

In this work, we present a detailed numerical investigation of continuous-time quantum walks applied to solving combinatorial optimization problems, using the Sherrington-Kirkpatrick spin glass ground state problem as a prototypical example. We generated 10k random problem instances for each of $n = 5$ through 20 qubit sizes. This corresponds to problem sizes of $N = 2^5$ to 2^{20}, since the ground state is one of $N = 2^n$ basis states. We use a random energy model (Derrida, 1980) for comparisons, to draw out the effects of the correlations in the spin glass. A highly ordered problem is easy to solve, like a spin system with all the spins lined up in the same direction. Likewise, a completely random problem is fully described by the average values, details of the exact spin configuration doesn't provide useful information. Intermediate problems with some structure are both hard and interesting, with complex behaviour and phase diagrams, like spin models with frustration and spin glass phases. Analogously, real optimisation problems have correlations that make them hard to solve but also produce interesting solutions.

The paper is structured as follows. In Section 2, we review the setting for computation by continuous-time quantum walk encoded into qubits, including application to the search problem. In Section 3, we introduce the Sherrington-Kirkpatrick spin glass model, and a related model we use for comparison. In Section 4, we describe the numerical methods used in this investigation. In Section 5, we present the main results showing that quantum walks can find spin glass ground states more efficiently than searching. In Section 6, we identify the computational mechanisms and important aspects of the problem structure that contribute to the effectiveness of quantum walk computation. Finally, in Section 7, we summarize and conclude.

2. Computing with quantum walks

Both discrete (coined) quantum walks and continuous-time quantum walks are used for computation (see, e.g., Shenvi et al., 2003; Lovett et al., 2019). This work only uses the continuous-time quantum walk, and also only as an *encoded* quantum walk, in which qubits are used to store the binary labels of the positions of the quantum walker.

2.1. Continuous-time quantum walks

A continuous-time quantum walk is defined on an undirected graph $G(V, E)$, with $V = \{j\}_{j=0}^{N-1}$ the set of N vertex labels and E the set of label-pairs (j, k) associated with edges. The adjacency matrix A of the graph has entries $A_{jk} = 1$ for $(j, k) \in E$ and $A_{jk} = 0$ otherwise. The Laplacian of G is $L = A - D$, where D is a diagonal matrix formed from the degree of each vertex, $D_{jj} = \deg(j)$, where $\deg(j)$ is the number of edges connected to vertex j. Both the adjacency matrix A and Laplacian L are symmetric matrices which can thus be used to define a quantum Hamiltonian for the dynamics of the continuous-time quantum walk on the graph. In this work, we only need regular graphs, for which $\deg(j)$ is constant with respect to j. For regular graphs, the only difference between using the adjacency matrix A or Laplacian L is an irrelevant global phase (Childs and Goldstone, 2004), however, we use the Laplacian form of the Hamiltonian for consistency with prior work. We thus define the quantum walk Hamiltonian $\hat{H}_G$ for a quantum walk on graph G by

$$\langle j| \hat{H}_G |k\rangle = -\gamma L_{jk}, \tag{5}$$

where γ is the hopping rate between connected vertices per unit time. The states $|j\rangle, |k\rangle$ for $j, k \in V$ are associated with the vertices of G and form a basis for a Hilbert space of dimension N. In the Ising model context, the dimension of the Hilbert space is $N = 2^n$ where n is the number of qubits, and $\{|j\rangle\}_{j=0}^{N-1}$ is the computational basis. For a quantum walk starting in state $|\psi(0)\rangle$, the state of the walker evolves according to the Schrödinger equation, with formal solution

$$|\psi(t)\rangle = \exp\{-\mathrm{i}\hat{H}_G t\} |\psi(0)\rangle, \tag{6}$$

using units in which $\hbar = 1$.

2.2. Computing using a quantum walk

The task is to solve an optimisation problem whose $N = 2^n$ candidate solutions are represented in the computational basis $\{|j\rangle\}_{j=0}^{N-1}$. The problem is encoded in an Ising Hamiltonian $\hat{H}_P$, of the form described by $\hat{H}_I$ in (1) and whose eigenbasis is the computational basis. We write the basis state with eigenvalue $E_j^{(P)}$ as $\left|E_j^{(P)}\right\rangle$, and adopt the convention that $E_j^{(P)} \leq E_{j+1}^{(P)}$. The encoding is chosen such that the actual solution corresponds to the ground-state $\left|E_0^{(P)}\right\rangle$ of the problem Hamiltonian $\hat{H}_P$.

To use a quantum walk to solve the problem, first choose a suitable state $|\psi(0)\rangle$ in which to initialize the system. With no prior knowledge of the solution, the equal superposition of all basis states

$$|\psi(0)\rangle = N^{-1/2} \sum_{j=0}^{N-1} |j\rangle, \tag{7}$$

is a sensible choice that avoids bias. More generally, the initial state $|\psi(0)\rangle$ can be prepared as weighted or biased superposition, to incorporate prior knowledge about the solution (Chancellor, 2017; Perdomo-Ortiz et al., 2011; Baldwin and Laumann, 2018).

Then, choose a suitable walk graph G. The main requirement is that the ground state of the quantum walk Hamiltonian $\hat{H}_G$ coincides with the initial state $|\psi(0)\rangle$.

The full Hamiltonian $\hat{H}(\gamma)$ is defined by adding the quantum walk Hamiltonian $\hat{H}_G$ to the problem Hamiltonian $\hat{H}_P$

$$\hat{H}(\gamma) \equiv \hat{H}_G + \hat{H}_P. \tag{8}$$

The computation is performed by evolving the initial state (7) under the full Hamiltonian $\hat{H}(\gamma)$ for a time t_f, then measuring the qubit register in the computational basis. The intuition is that the quantum walk dynamics provide rapid exploration of the basis states, while the energy structure of the problem Hamiltonian $\hat{H}_P$ causes localization around low-energy states.

The success probability $P(t_f) = \left|\left\langle E_0^{(P)} \middle| \psi(t_f) \right\rangle\right|^2$ of finding the solution state when measuring will not in general be unity. It will typically be necessary to repeat the protocol multiples times to obtain a high probability of success over all the repeats. In general, it will be best to use different measurement times t_f for each repeat. Different measurement times will produce different success probabilities $P(t_f)$, and varying the measurement time avoids repeatedly measuring at a time for which the probability $P(t_f)$ happens to be atypically small. More precisely, choose the measurement time t_f uniformly at random in an interval $[t, t+\Delta t]$, and define an average success probability

$$\bar{P}(t, \Delta t) \equiv \frac{1}{\Delta t} \int_t^{t+\Delta t} \mathrm{d}t_f P(t_f). \tag{9}$$

Operationally, choosing the measurement time t_f randomly in the interval $[t, t+\Delta t]$ samples success probabilities from the distribution with $\bar{P}(t, \Delta t)$ as its mean. Drawing measurement times in this way means that the protocol will typically need to be repeated at least $M_{\text{rep}} \sim 1/\bar{P}(t, \Delta t)$ times to achieve an overall $O(1)$ success probability. In the limit of small interval width Δt, the average success probability reduces to the single time probability $P(t_f) = \lim_{\Delta t \to 0} \bar{P}(t_f, \Delta t)$. The long time limit

$$P_\infty \equiv \bar{P}(0, \infty) \equiv \lim_{\Delta t \to \infty} \bar{P}(0, \Delta t) \tag{10}$$

is particularly useful as it can be calculated via a numerical diagonalization of the Hamiltonian (see section 4).

2.3. Graph choice for quantum walk computing

There are many graph-based Hamiltonians with the initial state $|\psi(0)\rangle$ defined in (7) as the ground state. A common choice is the *complete graph* K, in which every vertex is connected to every other. This graph has the quantum walk Hamiltonian $\hat{H}_K$ that couples every computational basis state $|j\rangle$ state to every other,

$$\begin{aligned} \hat{H}_K &= \gamma \left[N\mathbb{1} - \sum_{j,k=0}^{N-1} |k\rangle \langle j| \right] \\ &= \gamma N \left[\mathbb{1} - |\psi(0)\rangle \langle \psi(0)| \right]. \end{aligned} \tag{11}$$

The complete graph is useful because it makes some algorithms analytically tractable (see, e.g., Childs and Goldstone, 2004). However, for implementation on qubit-based hardware, the complete graph is not in general practical, requiring higher order interaction terms than the transverse Ising term (3). In this qubit setting, an implementation of the complete graph requires a sum over every one-body term (e.g $\hat{X}_j$), every two-body term (e.g $\hat{X}_j\hat{X}_k$), every three-body term (e.g $\hat{X}_j\hat{X}_k\hat{X}_l$) ...

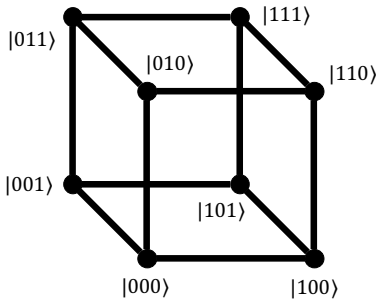

Figure 1. A 3-dimensional hypercube (a cube) graph in which the vertices represent 3-qubit computational basis states and the edges connect those states with Hamming distance 1.

up to the n-body term $\prod_{j=0}^{n-1} \hat{X}_j$, for a total of N terms. One- and two-body terms are relatively easy to implement, since they correspond to Hamiltonians found naturally. Terms in three or more Pauli-X operators are much more difficult and generally require extra qubits to engineer in real physical systems.

A more natural choice of graph for qubits is the hypercube. The n-bit labels are associated with the vertices of the graph such that the edges correspond to flipping one bit, as illustrated in figure 1. The hypercube quantum walk Hamiltonian $\hat{H}_h$ on n qubits is composed of single-body terms

$$\hat{H}_h = \gamma \left[n\mathbb{1} - \sum_{j=0}^{n-1} \hat{X}_j \right]. \tag{12}$$

With $\hat{H}_h$ as the graph Hamiltonian, the full quantum walk computational Hamiltonian $\hat{H}(\gamma)$ defined in (8) is a transverse Ising Hamiltonian in the form of $\hat{H}_{\mathrm{TIM}}$ in (4), with the control functions $A(t)$ and $B(t)$ kept constant throughout the computation. In this work, we predominantly use the hypercube graph, with some comparisons made with the same problems on the complete graph.

2.4. The search problem with quantum walks

The simplest example of an algorithm in this continuous-time quantum walk setting is the search problem, shown to have a quantum algorithm with a speed up over classical algorithms by Grover (1996). The problem is to find a single bit-string $m \in \{0,1\}^n$ out of $N = 2^n$ possible bit strings. To map this problem to the Ising Hamiltonian setting, the marked basis state $|m\rangle$ is given one less unit of energy than all the rest of the basis states, by defining the problem Hamiltonian $\hat{H}_{\mathrm{S}}$ as

$$\hat{H}_{\mathrm{S}} = -|m\rangle\langle m|. \tag{13}$$

By construction, the problem Hamiltonian $\hat{H}_{\mathrm{S}}$ has the marked state $|m\rangle$ as its ground state.

The continuous-time quantum walk search problem has been analytically solved (Childs and Goldstone, 2004) for several choices of walk graph. For the complete graph and the hypercube graph, a quantum speed up is obtained for carefully chosen optimal values of the hopping rate γ. For the complete graph Hamiltonian $\hat{H}_K$ the

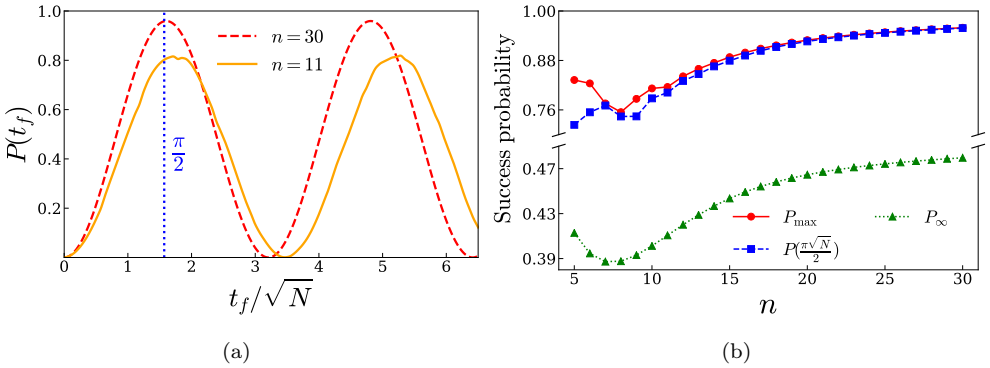

Figure 2. The search problem solved using a continuous-time quantum walk on the hypercube using the optimal hopping rate $\gamma_{\text{opt}}^{(h)}$ given by (14). (a) The probability $P(t_f)$ that a measurement at time t_f results in successfully finding the marked state $|m\rangle$ for two different numbers $n = 30$ (red, dashed line) and $n = 11$ (orange, solid line) of qubits (i.e problem sizes $N = 2^{30}$ and $N = 2^{11}$ respectively). (b) Comparison of instantaneous success probabilities $P(t_f)$, at the asymptotically optimal (blue squares, dashed line) and numerically determined best (red circles, solid line) measurement times t_f, and the infinite time average success probability P_∞ (green triangles, dotted line) defined in (10).

optimal value is $\gamma_{\text{opt}}^{(K)} = 1/N$, while for the hypercube Hamiltonian, $\hat{H}_h$, the optimal hopping rate $\gamma_{\text{opt}}^{(h)}$ satisfies the relation

$$2\gamma_{\text{opt}}^{(h)} = \frac{1}{N}\sum_{r=1}^{n}\binom{n}{r}\frac{1}{r} \tag{14}$$

where $\binom{n}{r} = \frac{n!}{r!(n-r!)}$ is the binomial coefficient. For a quantum speed up, the hopping rate must be set to $\gamma_{\text{opt}}^{(h)}$ defined by (14) with high precision. It has been shown (Morley et al., 2019) that the fractional tolerance to misspecification of the optimal hopping rate $\gamma_{\text{opt}}^{(h)}$ falls as $O(N^{-1/2})$.

The measurement time must also be chosen appropriately. In the limit of large problem size N, the marked state can be found with unit success probability, $\lim_{N\to\infty}\left[P(t_f^{(\text{opt})})\right] = 1$, by measuring in the computational basis at an optimal measurement time $t_f^{(\text{opt})}$. For both the hypercube and complete graphs, the optimal time $t_f^{(\text{opt})}$ scales with the square-root of the problem size N as $t_f^{(\text{opt})} \simeq \frac{\pi}{2}N^{-1/2}$. This corresponds to a quadratic speedup compared to the best classical approach, which has been proven to the best possible speedup (Bennett et al., 1997).

The variation of $P(t_f)$ with t_f is shown in figure 2(a) for search on hypercube graphs of size $N = 2^{30}$ (i.e., $n = 30$ qubits) and $N = 2^{11}$ (i.e., $n = 11$ qubits), using the optimal hopping rate $\gamma_{\text{opt}}^{(h)}$. The sinusoidal oscillations of the probability $P(t_f)$ occur because the quantum walk is performing Rabi oscillations between the initial state and the marked state. The two lowest energy levels of the full Hamiltonian $\hat{H}(\gamma_{\text{opt}}^{(h)})$ undergo an avoided level crossing, and the associated eigenstates $\left|E_0(\gamma_{\text{opt}}^{(h)}\right\rangle)$ and $\left|E_1(\gamma_{\text{opt}}^{(h)}\right\rangle)$ are approximately the orthogonal equal superpositions of the starting

state and marked state, $\left|E_{0,1}(\gamma^{(h)}_{\text{opt}}\right\rangle) \simeq (|\psi(0)\rangle \pm |m\rangle)/\sqrt{2}$. The gap $E_1(\gamma^{(h)}_{\text{opt}}) - E_0(\gamma^{(h)}_{\text{opt}})$ scales with the problem size N as $O(N^{-1/2})$ (Childs and Goldstone, 2004).

These simple, two-level dynamics describe the quantum walk solution to the search problem well for large problem size N: the oscillations in the $N = 2^{30}$ case have no visible irregularities. For smaller sizes, finite-size effects due to population of higher energy levels are apparent: the oscillations in the $N = 2^{11}$ case have lower probability peaks and show some irregular behaviour, such as the small dip on the first peak. These finite-size effects are further illustrated in figure 2(b), which shows the instantaneous success probability $P(t_f)$ at the asymptotically optimal and numerically determined best times, as well as the infinite-time average success probability P_∞ defined in (10). All three probabilities show a pronounced dip around $n = 8$ qubits, with smooth behaviour only settling in for $n > 12$ qubits. Figure 2(b) also shows that the infinite-time probability P_∞ asymptotes to a half. Hence, a quantum walk search with a random measurement times should on average only need to be repeated twice to locate the marked state; knowing the exact time to measure for the optimal success probability is not necessary for the success of the algorithm.

The search problem in the qubit setting has two important drawbacks. Firstly, implementing the problem Hamiltonian $\hat{H}_S$ directly on n qubits requires $O(2^N)$ terms of products of up to n Pauli-Z operators, similar to the problem with implementing the complete-graph Hamiltonian $\hat{H}_K$, defined in (11), on qubits. There are methods to overcome this for permutation-symmetric problems like search, at a cost of using additional qubits to create gadgets (Chancellor et al., 2017, 2016; Dodds et al., 2018). Secondly, it is impossible to map the problem Hamiltonian to qubits without specifying the solution outright. Hence, the search problem serves as a useful toy problem, especially in contexts where having analytic, computational, and physical implementations available for comparisons facilitates benchmarking and other testbed processes.

3. Spin glass problem definitions

In this work we focus on spin glass problems that have features in common with real life hard optimisations problems and, unlike the search problem, do not admit analytic solutions. The search problem solved by quantum walk provides useful comparisons with these spin glass problems.

3.1. Sherrington-Kirkpatrick spin glass

The Sherrington-Kirkpatrick (SK) spin glass Hamiltonian H_{SK} (Sherrington and Kirkpatrick, 1975) is defined on n spins as

$$H_{\text{SK}} = -\frac{1}{2} \sum_{(j \neq k)=0}^{n-1} J_{jk} S_j S_k \tag{15}$$

where S_j are the classical spins ($S_j \in \{-1, 1\}$) and the couplings J_{jk} are drawn independently from the normal distribution $\mathcal{N}(\mu, \sigma^2_{\text{SK}})$ with mean μ and variance σ^2_{SK}. Finding the ground state of this Hamiltonian is NP-Hard (Choi, 2010), and *uniformly* hard, due to its finite-temperature phase transition (Sherrington and Kirkpatrick, 1975).

It is computationally convenient to break the spin inversion symmetry by adding single-body field terms of the form $\sum_{j=0}^{n-1} h_j S_k$, where h_j are the field strength values. Like the couplings J_{jk}, the fields h_j are also drawn independently from $\mathcal{N}(\mu, \sigma_{\mathrm{SK}}^2)$. When the fields strengths h_j are drawn from the same distribution as the coupling strengths J_{jk}, the hardness of finding the ground state follows directly from the hardness of the $h_j = 0$ case. The SK spin glass with such fields is mathematically equivalent to a zero field spin glass with one more spin which is "fixed" in one orientation. This is not true in general for different distributions of field strength h_j. There are known examples in which fields can destroy spin glass behaviour (see, e.g., Feng et al., 2014; Young and Katzgraber, 2004). In particular, if the field strengths are much larger than the coupling strengths ($h_j \gg J_{jk}$ for all j, k), then the energy is minimized trivially when all the spins each minimize the energy with respect to their individual fields. While the distribution of field strengths could be used to tune the problem hardness, we do not use it in this way here, and only consider cases where the field and coupling strengths are drawn from the same distribution.

The mapping into the quantum Ising model is almost trivial: the classical spin variables S_j are simply mapped to Pauli-Z operators. Thus, the problem Hamiltonian $\hat{H}_{\mathrm{SK}}$ becomes

$$\hat{H}_{\mathrm{SK}} = -\frac{1}{2} \sum_{(j \neq k)=0}^{n-1} J_{jk} \hat{Z}_j \hat{Z}_k - \sum_{j=0}^{n-1} h_j \hat{Z}_j, \tag{16}$$

The SK problem Hamiltonian differs from the search problem by having structure: the covariance between the energies of two basis states depends on the Hamming-distance between them (Baldwin and Laumann, 2018). Knowing the energy of one state gives some information about the energy of states that differ by a small number of bit-flips. This results in a distribution of the eigenenergies that is almost normal, as can be seen by plotting the distributions and numerically calculating moments, but which deviates from normal in the tails of the distribution.

3.2. Random energy model

To isolate the effect of the Hamming-distance structure in the SK problem, we compare it with the random energy model (REM) (Derrida, 1980), in which the eigenenergies themselves are independently drawn from a normal distribution. The problem Hamiltonian $\hat{H}_{\mathrm{REM}}$ for REM is

$$\hat{H}_{\mathrm{REM}} = \sum_{j=0}^{N-1} F_j \left|j\right\rangle \left\langle j\right|, \tag{17}$$

with $\{|j\rangle\}_{j=0}^{N-1}$ the computational (Z) basis and the energies F_j drawn independently from the normal distribution $\mathcal{N}(0, \sigma_{\mathrm{REM}}^2)$.

REM has a similar energy level distribution to that of SK, apart from the tails. By definition it lacks the correlations: knowing the energy of one state gives no information about the energies of other states. Comparison between these two models highlights the effect of the correlated structure in the SK model.

4. Numerical methods

The main tool used for the investigations in this work is numerical simulation. We are studying computationally hard problems for which there are no tractable analytical

solutions except in special cases.

For each number of qubits $5 \leq n \leq 20$ we generated 10,000 instances of the SK spin glass Hamiltonian, defined in (16), with the couplings J_{jk} and fields h_j drawn with a standard deviation $\sigma_{\mathrm{SK}} = \omega_{\mathrm{SK}}$, where ω_{SK} is an arbitrary energy unit. The value $\omega_{\mathrm{SK}} = 5$ was used for computational convenience, but choosing any arbitrary constant will only affect overall time and energy scales by a constant factor. The energy unit ω_{SK} has been scaled out of the plots where relevant. We also generated 10,000 instances of the REM Hamiltonian, defined in (17), for each number of qubits $5 \leq n \leq 15$, with normally-distributed energies F_j drawn with a standard deviation $\sigma_{\mathrm{REM}} = \omega_{\mathrm{REM}}$. The value $\omega_{\mathrm{REM}} = 1$ was used for computational convenience, but choosing any arbitrary constant will only affect overall time and energy scales by a constant factor.

The key quantity to determine numerically is the probability that the ground state is found by running a quantum walk computation on each spin glass instance. It is particularly convenient to compute the infinite-time probability P_∞ given by (20) for sizes where full diagonalization is possible. Writing the spectral expansion of the full computational quantum walk Hamiltonian as

$$\hat{H}(\gamma) = \sum_{j=0}^{N-1} E_j(\gamma) \left|E_j(\gamma)\right\rangle \left\langle E_j(\gamma)\right|, \tag{18}$$

with indices ordered such that $E_j(\gamma) \leq E_{j+1}(\gamma)$ and $|E_j(\gamma)\rangle$ the eigenstate with eigenvalue $E_j(\gamma)$, we can write the instantaneous probability in terms of the spectral expansions as

$$\begin{aligned} P(t) &= \left|\left\langle E_0^{(P)}\right| \exp\left(-it\hat{H}(\gamma)\right) |\psi(0)\rangle\right|^2 \\ &= \left|\sum_{a=0}^{N-1} \exp\left(-itE_a\right) \left\langle E_0^{(P)}\middle|E_a(\gamma)\right\rangle \langle E_a(\gamma)|\psi(0)\rangle\right|^2 \\ &= \sum_{a=0}^{N-1} \left|\left\langle E_0^{(P)}\middle|E_a(\gamma)\right\rangle\right|^2 + \left|\langle E_a(\gamma)|\psi(0)\rangle\right|^2 \\ &\quad \sum_{a,b=0}^{N-1} \left[\exp\left(-it(E_a - E_b)\right) \left\langle E_0^{(P)}\middle|E_a(\gamma)\right\rangle \times \right. \\ &\quad \left. \langle E_a(\gamma)|\psi(0)\rangle \left\langle E_b(\gamma)\middle|E_0^{(P)}\right\rangle \langle\psi(0)|E_b(\gamma)\rangle\right]. \end{aligned} \tag{19}$$

Assuming rationally-independent gaps $E_a - E_b$, and no degeneracy, which is justified for the randomized nature of the SK and REM problems, the oscillatory terms vanish in the infinite limit to leave the infinite time probability P_∞ given by

$$P_\infty = \sum_{a=0}^{N-1} \left|\left\langle E_0^{(P)}\middle|E_a(\gamma)\right\rangle\right|^2 \left|\langle E_a(\gamma)|\psi(0)\rangle\right|^2. \tag{20}$$

All of the numerical simulation in this work has been performed using the Python3 language (Van Rossum and Drake, 2003), aided extensively by the IPython (Perez and Granger, 2007) interpreter and the Jupyter Notebook (Kluyver et al., 2016) system. The numerical heavy-lifting has been done using NumPy (Oliphant, 2006), SciPy (Jones et al., 2001–), and pandas (McKinney et al., 2010), and the plotting has

been done using matplotlib (Hunter, 2007). The dynamical simulations have been performed by computing the action of the propagator $\exp(-it\hat{H}(\gamma))$ on the initial state $|\psi(0)\rangle$, using the sparse matrix functions within SciPy when possible. Where relevant, figures in this paper have error bars included. However, in most cases the error bars are much smaller than the size of the marker symbols used and so are not visible. This is due to the size of the datasets (10k instances per value of n), which provides a good level of accuracy for the average quantities.

Simulations were run on the Imperial high performance computing facility. The data for all the instances used will soon be available on a permanent data archive. In the meantime, the data are available from the authors upon request.

5. Quantum walks with spin glasses

In order to implement a quantum walk algorithm for finding the ground states of the spin glasses defined in section 3, we follow the procedure described in section 2.2: choose a quantum walk graph G and associated Hamiltonian $\hat{H}_G$, and add the spin glass Hamiltonian to get the full computational quantum walk Hamiltonian,

$$\hat{H}(\gamma) = \hat{H}_G + \hat{H}_P, \tag{21}$$

where $\hat{H}_P$ refers to $\hat{H}_{\mathrm{SK}}$ or $\hat{H}_{\mathrm{REM}}$ as appropriate.

Since the hypercube is the natural choice of graph for qubit implementations, we use this graph, with quantum walk Hamiltonian $\hat{H}_h$ defined in (12), for most of this work, unless otherwise indicated. For the initial state $|\psi(0)\rangle$, we use the equal superposition (7), which is the ground state of the hypercube Hamiltonian $\hat{H}_h$.

5.1. Setting the hopping rate

Unlike the search problem, for SK and REM it is impossible to efficiently calculate the optimal hopping rate $\gamma_{\mathrm{opt}}^{(h)}$ that maximizes the success probability. Some plots of the infinite-time probability P_∞ against hopping rate γ for typical 11-qubit examples of the SK and REM are shown in figure 3. Note that the maximal success probability varies by an order of magnitude between the two problem-types, with REM highest and SK lowest. In these plots, it can be seen that, while the optimal hopping rate $\gamma_{\mathrm{opt}}^{(h)}$ is instance-dependent, the dependence of infinite-time probability P_∞ on hopping rate γ is typically characterized by broad, bumpy peaks for SK, and by narrow, well-defined peaks for REM. This indicates that, while a precise value of the hopping rate γ is needed for REM, there is some tolerance to non-optimal values of the hopping rate γ for SK.

To investigate the optimal success probability more systematically, we performed a brute-force numerical search to find the optimal hopping rate $\gamma_{\mathrm{opt}}^{(h)}$ that maximizes the success probability P_∞ for each spin glass instance from the datasets of 10k random instances. This gives a baseline maximum single-shot success probability for the quantum walk algorithm.

The optimal hopping rates $\gamma_{\mathrm{opt}}^{(h)}$ correspond to the best a quantum walk algorithm on the hypercube can possibly do. For practical algorithms, we need a heuristic method for choosing the hopping rate that can be calculated from the known parameters. Guided by the quantum walk search algorithm for which the optimal hopping rate balances the energy between the two components of the Hamiltonian, $\hat{H}_P$ and $\hat{H}_G$, we define the heuristic hopping rate $\gamma_{\mathrm{heur}}^{(h)}$ for SK and REM such

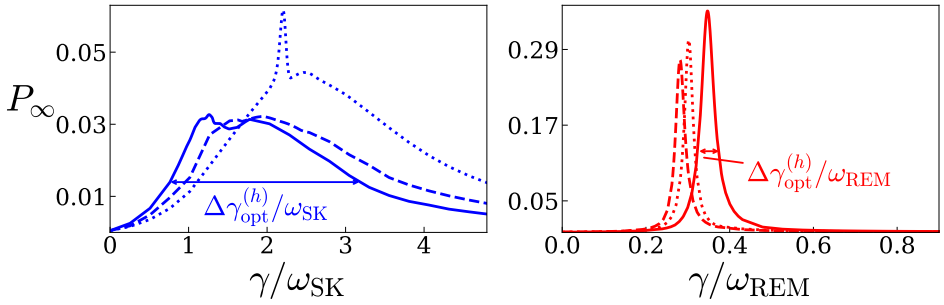

Figure 3. Infinite-time success probability P_∞ against hopping rate γ scaled by the energy unit ω_P for 3 typical 11-qubit examples of SK (left) and REM (right). Also indicated (for one example in each plot) is the width $\Delta\gamma^{(h)}_{\rm opt}$ of the peak (also scaled by ω_P).

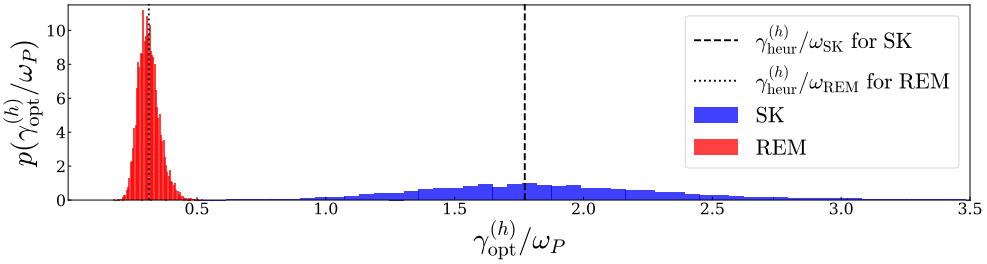

Figure 4. Histograms of the numerically-found optimal hopping rates $\gamma^{(h)}_{\rm opt}$ scaled by the energy unit ω_P for the 10,000 11-qubit instances of SK (blue) and REM (red). The dashed and dotted lines show the heuristic hopping rate $\gamma^{(h)}_{\rm heur}$, calculated according to (22), for SK and REM respectively (also scaled by ω_P).

that it balances these overall energy-scales. In particular, at each number of qubits n we choose to match the energy-spread $E^{(h)}_{N-1} - E^{(h)}_0$ of the hypercube quantum walk Hamiltonian $\hat{H}_h$ with the *average* energy-spread $\langle E^{(P)}_{N-1} - E^{(P)}_0 \rangle$ of the problem Hamiltonian $\hat{H}_P$. For the hypercube Hamiltonian $\hat{H}_h$ defined in (12), we have the energy spread $E^{(h)}_{N-1} - E^{(h)}_0 = 2n\gamma$; hence, we define the heuristic hopping rate $\gamma^{(h)}_{\rm heur}$ by

$$\gamma^{(h)}_{\rm heur} \equiv \frac{1}{2n}\left\langle E^{(P)}_{N-1} - E^{(P)}_0 \right\rangle. \tag{22}$$

To show that this heuristic is sensible, we show in figure 4, for the 11-qubit data set, the distributions of optimal hopping rates $\gamma^{(h)}_{\rm opt}$ for SK (blue) and REM (red), as well as the heuristic hopping rates (black, dashed and dotted lines for SK and REM respectively) calculated according to (22). For both SK and REM, the heuristic hopping rate $\gamma^{(h)}_{\rm heur}$ falls in the centre of the $\gamma^{(h)}_{\rm opt}$ distributions.

For a normal distribution of energy levels, the average problem energy spread can be estimated as

$$\left\langle E^{(P)}_{N-1} - E^{(P)}_0 \right\rangle \simeq -(2\sqrt{2}\sigma^{(\rm energy)}_P)\,{\rm erf}^{-1}\left(\frac{1}{N} - 1\right), \tag{23}$$

where $\sigma_P^{(\text{energy})}$ is the standard deviation of the energy eigenvalues of the problem Hamiltonian. For REM, the standard deviation $\sigma_{\text{REM}}^{(\text{energy})}$ is equal to the energy unit ω_{REM} by definition (see section 3.2). For SK, the standard deviation $\sigma_{\text{SK}}^{(\text{energy})}$ can be shown to be equal to $\frac{\omega_{\text{SK}}}{2}\sqrt{n(n+3)}$. Equation (23) is accurate for REM (which has normally-distributed energy levels by definition) but, as already noted, the distribution of the eigenenergies in SK deviates from normal, especially in the tails. Numerically, we find that there is a multiplicative constant factor of approximately 0.887 that corrects the formula in (23) for SK for the effects of the non-normal tails. For the numerical analysis, we use the numerically calculated average energy-spread at each number of qubits n.

Figure 5(a) compares the heuristic hopping rate $\gamma_{\text{heur}}^{(h)}$ and average optimal hopping rate $\langle\gamma_{\text{opt}}^{(h)}\rangle$ at different numbers of qubits n. The full width at half maximum (FWHM) has also been calculated for each instance to estimate the the tolerance $\Delta\gamma_{\text{opt}}^{(h)}$ to deviations from the optimal hopping rate $\gamma_{\text{opt}}^{(h)}$ (illustrated in figure 3). The width of the shaded regions in figure 5(a) corresponds to the average tolerance range $\langle\Delta\gamma_{\text{opt}}^{(h)}\rangle$ at each number n of qubits. While the heuristic hopping rate differs slightly from the the average optimal hopping rate for SK, the average tolerance range $\langle\Delta\gamma_{\text{opt}}^{(h)}\rangle$ is much broader, and does not shrink with increasing number of qubits n. For REM, however, while we see close agreement on average, the tolerance range shrinks quickly with the number of qubits n as the peaks (as in figure 3, right) become narrower. This means that the heuristic hopping rate $\gamma_{\text{heur}}^{(h)}$ is more likely to lie outside of the actual probability peak for each instance, even though it agrees well with the average optimal hopping rate $\langle\gamma_{\text{opt}}^{(h)}\rangle$. Hence, a quantum walk with the heuristic hopping rate $\gamma_{\text{heur}}^{(h)}$ does not perform well for most REM instances.

It is instructive to quantify this sensitivity to deviations from the optimal hopping rate $\gamma_{\text{opt}}^{(h)}$. Figure 5(b) shows log-linear and log-log plots of the average *fractional* tolerance range $\langle\Delta\gamma_{\text{opt}}^{(h)}/\gamma_{\text{opt}}^{(h)}\rangle$ against number n of qubits for SK (blue circles), REM (red squares) and search (green triangles) on the hypercube.

For SK, the fractional tolerance range $\langle\Delta\gamma_{\text{opt}}^{(h)}/\gamma_{\text{opt}}^{(h)}\rangle$ decreases as approximately $1/n$, while for REM and search the decrease is approximately $N^{-0.5}$. This decrease is expected theoretically for search (Childs and Goldstone, 2004). The fitted lines do not show exactly a square-root dependence (exponent of -0.5) due to the finite size effects for small numbers of qubits $n \leq 12$. Thus we see that REM behaves like the search problem in a quantum walk setting. For a precisely optimal hopping rate $\gamma_{\text{opt}}^{(h)}$, the success probability is high, but this instance-dependent hopping rate that is hard to predict, unlike for the analytically tractable quantum walk search algorithm. Without this precise hopping rate, quantum walks perform no better than guessing for the search problem and for REM. In contrast, quantum walk computation for SK gives a better-than-guessing success probability $P_\infty > 1/N$ for the heuristic hopping rate $\gamma_{\text{heur}}^{(h)}$ calculated according to (22).

With the conditions under which we can achieve a better-than-guessing success probability understood, we turn to the scaling of this success probability with problem size N.

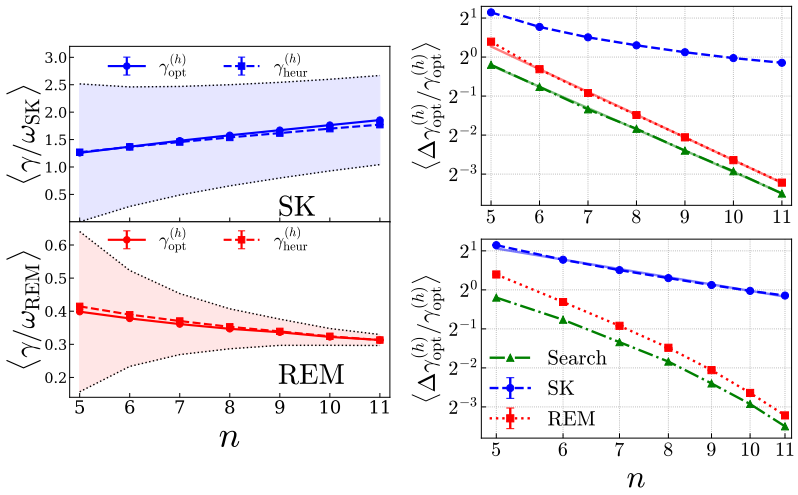

(a) (b)

Figure 5. (a) Average optimal (circles, solid line) and heuristic (squares, dashed line) hopping rates, $\langle\gamma_{\rm opt}^{(h)}\rangle$ and $\gamma_{\rm heur}^{(h)}$, against number n of qubits for SK (top, blue) and REM (bottom, red). The shaded regions enclosed by dotted lines indicate the average tolerance range $\langle\Delta\gamma_{\rm opt}^{(h)}\rangle$ to non-optimal hopping rates (defined as full width at half maximum (FWHM) of the probability peak surrounding $\gamma_{\rm opt}^{(h)}$, as illustrated in figure 3). (b) Log-linear plot (top) and log-log plot (bottom) of average *fractional* tolerance range $\langle\Delta\gamma_{\rm opt}^{(h)}/\gamma_{\rm opt}^{(h)}\rangle$. REM (red squares, dotted line) shows an exponential decrease, fitting to a line (red, solid line) with a gradient of -0.583 ± 0.006 in the log-linear plot. SK (blue circles, dotted line) shows a polynomial decrease, fitting to a line (solid blue) in the log-log plot with a gradient of -1.09 ± 0.04. The same quantity for the search problem calculated the same way is also shown (green triangles, dash-dotted line), and it fits well to a line (solid green) in the log-linear plot with a gradient of -0.546 ± 0.004.

5.2. Success probability

Figure 6 shows how the single-time success-probability $P(t_f)$ varies with the measurement time t_f for two typical 11-qubit examples of SK and REM. In the REM case, the behaviour is similar to that shown in figure 2(a) for search: an oscillatory nature indicating the dominance of a two-level avoided-crossing feature, but with evidence of the population of other energy-levels that lead to finite-size effects in search. For REM, these finite-size effects are more pronounced, and are instance-dependent. The random nature of the REM problems means there is not such a clear cut off size, as there is for the search problem, above which finite size effects are negligible. In the SK case, the behaviour is quite different from search or REM: there is no indication of dominant oscillatory behaviour; instead, these plots show unpredictable, highly instance-dependent fluctuating dynamics for all the sizes we are using. This indicates that, for SK, the behaviour is dominated by the excitation of many energy levels.

For both REM and SK, there is no simple way to define a single optimal measurement time $t_f^{(\rm opt)}$. As already noted for the search problem, this can be

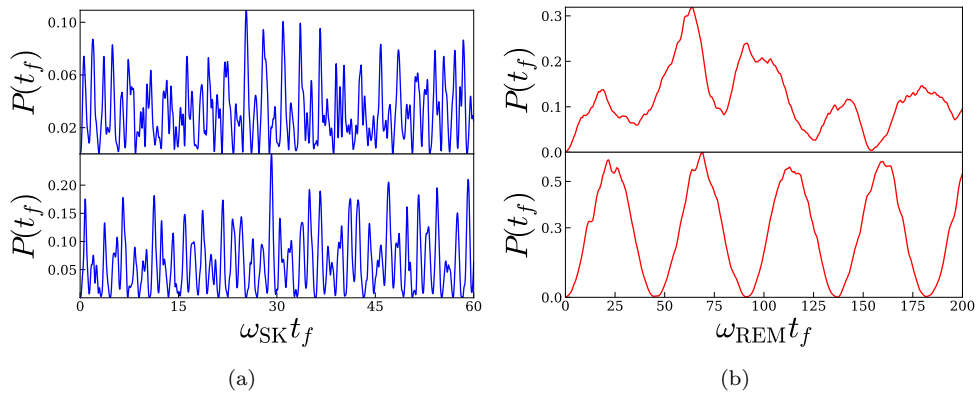

Figure 6. Instantaneous success probability $P(t_f)$ against dimensionless measurement time $\omega_P t_f$ for quantum walk on 2 typical 11-qubit SK examples (a) and for 2 typical 11-qubit REM examples (b).

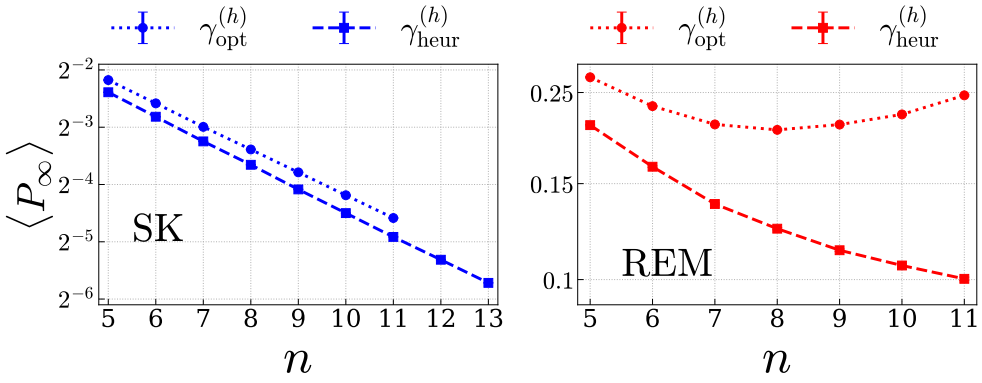

Figure 7. Blue, left: Log-linear plot of average infinite time success probability $\langle P_\infty \rangle$ against number of qubits n for SK, using optimal (circles, dotted line) and heuristic (squares, dashed line) hopping rates $\gamma^{(h)}_{\mathrm{opt}}$ and $\gamma^{(h)}_{\mathrm{opt}}$. The dependence of probability on number of qubits is $\sim \tilde{O}(N^{0.4})$ in both cases, being only slightly worse for the heuristic rate. Red, right: Linear-linear plot of the same quantities for REM. In this case, the probability stays at constant order for the optimal rate and decays for the heuristic rate.

handled by using the time averaged probabilities defined in (9). We first consider the infinite-time probability P_∞, as defined in (10), since it is easy to calculate (see Section 4). The infinite-time probability P_∞ estimates a lower bound on the number of repeats necessary on average to achieve $O(1)$ success probability. Figure 7 shows the average infinite-time probability $\langle P_\infty \rangle$ against the number n of qubits for the two problems in both the optimal $\gamma^{(h)}_{\mathrm{opt}}$ and heuristic $\gamma^{(h)}_{\mathrm{heur}}$ hopping rates. For SK, this gives exponential decay with number of qubits in both cases: the average probability $\langle P_\infty \rangle$ changes with number of qubits n according to the numerically-determined relationships $\log_2\langle P_\infty \rangle = (-0.402 \pm 0.001)n + (-0.174 \pm 0.008)$ and $\log_2\langle P_\infty \rangle = (-0.417 \pm 0.002)n + (-0.32 \pm 0.01)$ with optimal $\gamma^{(h)}_{\mathrm{opt}}$ and heuristic $\gamma^{(h)}_{\mathrm{heur}}$

hopping rates respectively. From this numerical analysis at small sizes $n \leq 13$, we can estimate the scalings

$$\langle P_\infty \rangle = \begin{array}{ll} \tilde{O}(N^{-0.402\pm0.001}) & \text{with } \gamma_{\text{opt}}^{(h)} \\ \tilde{O}(N^{-0.417\pm0.002}) & \text{with } \gamma_{\text{heur}}^{(h)} \end{array} , \tag{24}$$

where $\tilde{O}$ may neglect factors logarithmic in its argument. That is, using the heuristic hopping rate $\gamma_{\text{heur}}^{(h)}$ instead of the optimal hopping rate $\gamma_{\text{opt}}^{(h)}$ has only a minor impact on the success-probability P_∞.

For REM, the behaviour is quite different. With the optimal hopping rate $\gamma_{\text{opt}}^{(h)}$ we see a success probability P_∞ of constant order but with a pronounced dip. This behaviour is similar to that seen for the search problem, where the dip seen in figure 2(b) is a finite-size effect. This similarity is expected, given the similarity between the dynamical behaviour shown in figure 2(a) for search and in figure 6(b) for REM. With the heuristic hopping rate $\gamma_{\text{heur}}^{(h)}$ for REM, we see a significantly reduced success-probability P_∞ compared to the optimal case. That is, the heuristic is performing poorly, despite the good agreement shown in figure 5(a).

The clear difference in behaviour between SK and REM can be explained by the different tolerances $\Delta\gamma_{\text{opt}}^{(h)}$ to deviations from the optimal hopping rate $\gamma_{\text{opt}}^{(h)}$ shown in figure 5(a) and figure 5(b). For SK, the tolerance range is broad enough for the heuristic to lie within it, while for REM the heuristic hopping rate $\gamma_{\text{heur}}^{(h)}$ almost always misses this range entirely even though it is close to the average optimal hopping rate $\left\langle \gamma_{\text{opt}}^{(h)} \right\rangle$.

5.3. Mixing times

We have thus numerically determined an average-case probability scaling with problem size N of $\sim \tilde{O}(N^{-0.42})$ for a quantum walk finding SK spin glass ground states, using the heuristic hopping rate $\gamma_{\text{heur}}^{(h)}$. This is based on the infinite time-success probability P_∞, i.e., uniform sampling from the distribution of all possible run times. We now investigate the time dependence in more detail: can we sample from a finite run time and still obtain the same speed up? We define a *mixing-time* $\tau_{\text{mix}}^{(\epsilon)}$ to be the latest time, t, for which the average probabilities $\bar{P}(0,t)$ and $\bar{P}(0,2t)$ at the two times t and $2t$ differ by a fraction greater than the fluctuation parameter ϵ,

$$\tau_{\text{mix}}^{(\epsilon)} = \max\{t : \left| \frac{\bar{P}(0,t) - \bar{P}(0,2t)}{\bar{P}(0,t)} \right| > \epsilon\}. \tag{25}$$

We numerically estimated the mixing-time $\tau_{\text{mix}}^{(0.05)}$ for each SK instance, using the optimal hopping rate $\gamma_{\text{opt}}^{(h)}$ for each instance. We simulated the quantum walk computation dynamics for a successively-doubling duration until a time at which the condition is met was reached. The fluctuation parameter $\epsilon = 0.05$ corresponds to a deviation of 5%. To verify that the mixing-time $\tau_{\text{mix}}^{(0.05)}$ correctly captures the relevant dynamical timescale, we also numerically estimated it for the search problem at each system size from $n = 5$ to $n = 30$ qubits. The mixing-time $\tau_{\text{mix}}^{(0.05)}$ for search produces the expected exponential timescale: the solid green line of best fit in figure 8(a) indicates that the mixing-time $\tau_{\text{mix}}^{(0.05)}$ changes with number n of qubits according to the relationship $\log_2 \tau_{\text{mix}}^{(0.05)} = (0.5000 \pm 0.0002)n + (3.424 \pm 0.006)$, giving the expected scaling with problem size N of $\tau_{\text{mix}}^{(0.05)} = \tilde{O}(N^{1/2})$. However, this only emerges at

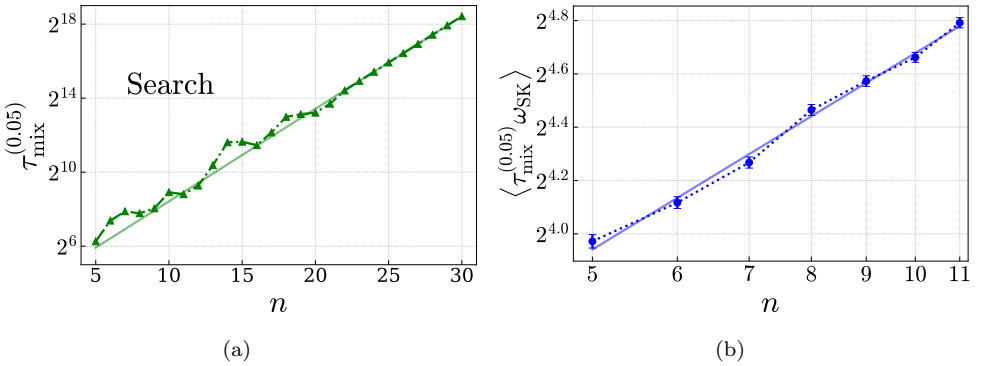

Figure 8. (a) Log-linear plot of the mixing time $\tau_{\rm mix}^{(0.05)}$ for search, using $\gamma_{\rm opt}^{(h)}$. The solid line of best fit indicates the expected scaling of $O(N^{0.5})$ at larger sizes, with finite-size effects dominating at small numbers of qubits $n \lesssim 20$. (b) Log-log plot of the avarage scaled mixing time $\langle \tau_{\rm mix}^{(0.05)} \omega_{\rm SK} \rangle$ against system-size n for SK, using $\gamma_{\rm opt}^{(h)}$. The solid line of best fit indicates a polynomial in n (logarithmic in problem size N) scaling of $\sim O(n^{0.75})$.

$n \sim 20$, below which the behaviour is dominated by the finite-size effects that arise due to population of higher energy levels.

Computational resources limited our estimates of the mixing time $\tau_{\rm mix}^{(0.05)}$ to a small number $n \leq 11$ of qubits. Unlike search, the SK behaviour is influenced by higher energy levels at all sizes. Hence, we do not expect to see significant finite-size effects as the behaviour is already close to typical at small sizes. In figure 8(b), we have scaled the mixing time $\tau_{\rm mix}^{(0.05)}$ by the energy unit $\omega_{\rm SK}$ to make a dimensionless quantity. Figure 8(b) shows a log-log plot of the scaled mixing-time averaged over the ensemble $\langle \tau_{\rm mix}^{(0.05)} \omega_{\rm SK} \rangle$. This average has a polynomial dependence on the number n of qubits for SK over these sizes: the solid blue line of best fit in figure 8(b) indicates that the mixing-time $\tau_{\rm mix}^{(0.05)}$ changes with the number n of qubits according to the relationship $\log_2 \langle \tau_{\rm mix}^{(0.05)} \omega_{\rm SK} \rangle = (0.74 \pm 0.03) \log_2 n + (2.23 \pm 0.08)$. This implies a logarithmic scaling with problem size N of

$$\langle \tau_{\rm mix}^{(0.05)} \omega_{\rm SK} \rangle = O(n^{0.74 \pm 0.03}) \simeq O([\log_2 N]^{0.75}). \tag{26}$$

Thus it contributes a logarithmic factor to the overall scaling.

To confirm the subsidiary nature of the time scaling for each SK run, we show in figure 9 a log-plot comparing, for the heuristic hopping rate $\gamma_{\rm heur}^{(h)}$, the success probability P_∞ in the infinite-time case (as in figure 7) and in the case of an early, logarithmically-scaling (with respect to N) measurement window $\frac{12.5\sqrt{n}}{\omega_{\rm SK}} \leq t \leq \frac{17.5\sqrt{n}}{\omega_{\rm SK}}$. This finite-time probability $\bar{P}(\frac{12.5\sqrt{n}}{\omega_{\rm SK}}, \frac{5.0\sqrt{n}}{\omega_{\rm SK}})$ is similar to the infinite-time probability P_∞: the solid purple line of best fit in figure 9 indicates that the average finite-time probability $\langle \bar{P}(\frac{12.5\sqrt{n}}{\omega_{\rm SK}}, \frac{5.0\sqrt{n}}{\omega_{\rm SK}}) \rangle$ changes with number of qubits n according to the relationship $\log_2 \langle \bar{P}^{\rm heur}(\frac{12.5\sqrt{n}}{\omega_{\rm SK}}, \frac{5.0\sqrt{n}}{\omega_{\rm SK}}) \rangle = (-0.410 \pm 0.002)n + (-0.37 \pm 0.02)$. This implies a scaling with problem size N of

$$\left\langle \bar{P}_{\rm heur}\left(\frac{12.5\sqrt{n}}{\omega_{\rm SK}}, \frac{5.0\sqrt{n}}{\omega_{\rm SK}}\right) \right\rangle = \tilde{O}(N^{-0.410 \pm 0.002}). \tag{27}$$

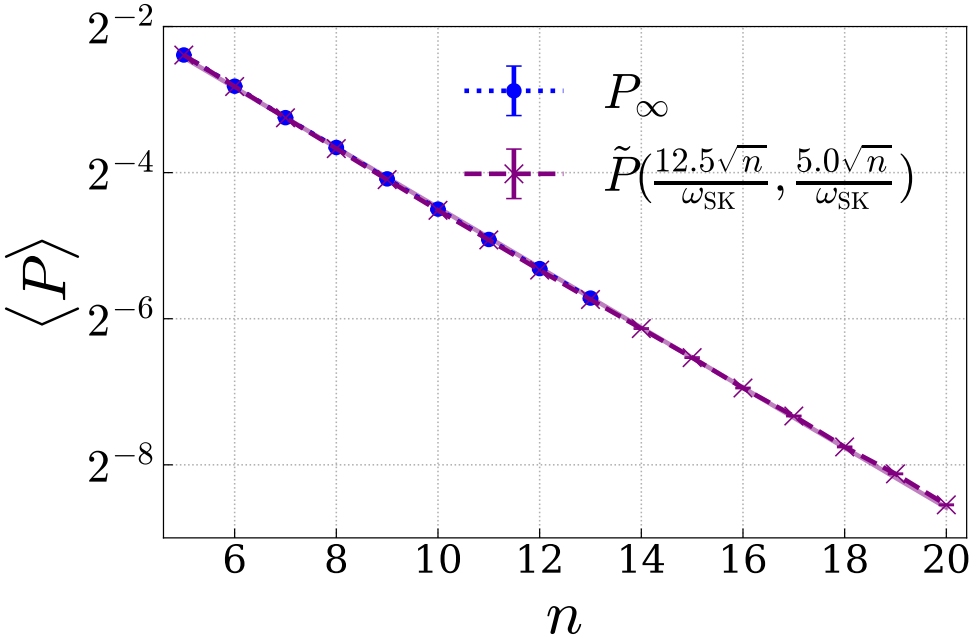

Figure 9. Log-plot of average success-probability using $\gamma^{(h)}_{\rm heur}$ against number of qubits in the infinite-time case (blue circles and dotted line) as in figure 7, and averaged just over the finite time-window between $t_{\rm min}\omega_{\rm SK} = 12.5\sqrt{n}$ and $t_{\rm ax}\omega_{\rm SK} = 17.5\sqrt{n}$ (purple crosses and dashed line). The decay in the finite-time case has exponent -0.410 ± 0.002 (from solid line of best fit), close to the -0.417 ± 0.002 in the infinite-time case.

This should be compared with (24), where the value of the exponent for *infinite-time* probability P_∞ with the heuristic hopping rate $\gamma^{(h)}_{\rm heur}$ is given by -0.417 ± 0.002. The required number of repeats for overall success probability $O(1)$ then translates into a time scaling of $\sim \tilde{O}(N^{0.41})$ in the average case.

These results constitute good numerical evidence for an average-case time-to-solution which scales with problem size N as $\sim \tilde{O}(N^{0.41})$ for using quantum walks to find spin glass ground states. This scaling is a better speed up, over classical guessing, than the best possible (quadratic, $O(N^{0.5})$) speed-up achievable for quantum walk search. Moreover, this comes without the requirement for exponential precision in setting the hopping rate that renders practical use of quantum walk searching difficult for large problems. We now present some insight into where the improvement over search comes from.

6. Computational mechanisms

6.1. Role of correlations in SK

To investigate whether the correlations of the energy with Hamming distance in SK play a significant role in the computational process of finding the ground state with a quantum walk, we performed three additional sets of numerical tests.

Firstly, we used the same SK instances but performed the quantum walk using

a complete graph Hamiltonian $\hat{H}_K$, defined in (11), instead of the hypercube graph Hamiltonian $\hat{H}_h$. This removes the correspondence of Hamming-distance between classical states with the distance between those states on the graph – for the complete graph, every state is one unit (edge) away from every other state. In terms of the Hamiltonian, the transverse Ising term is replaced by sums of products of up to n Pauli-X operators that flip up to n qubits at the same time, in all possible combinations. For each SK instance, we estimated the optimal hopping rate $\gamma_{\text{opt}}^{(K)}$ for the complete graph, and then used it to calculate the infinite-time probability P_∞.

Secondly, we constructed 'scrambled SK' instances, denoted sSK, by randomizing which state corresponds to which energy in the SK instances. In doing so, we arrive at Hamiltonians with identical energy spectra to the SK instances, but without the correlations between energy difference and Hamming distance on the hypercube graph. This approach has similarities with previous work (Farhi et al., 2010, 2008). For each sSK instance, we estimated the optimal hopping rate $\gamma_{\text{opt}}^{(h)}$, which is different from that used for the ordinary SK versions. This hopping rate was then used to calculate P_∞.

Thirdly, we sorted the eigenenergies of each REM instance in increasing size and assigned them to the computational basis states in the order of a binary-reflected Gray code on their bitstrings, to arrive at a problem denoted REMGC. In doing so, we added some amount of Hamming-distance structure by ensuring that the closest energies are assigned to states that differ by only a single bit-flip. For each REMGC instance, we have estimated an optimal hopping rate $\gamma_{\text{opt}}^{(h)}$, which is different from that used for the ordinary REM problem. Again, this was used to calculate the infinite-time probability P_∞. While REMGC is not a hard problem as defined, it provides a useful example to compare with how the quantum walk finds the ground state of a SK spin glass.

These three variants provide separate tests of the influence of the graph structure (choice of quantum walk Hamiltonian) and problem structure (pairwise correlations in SK). Figure 10 shows how the infinite-time probability P_∞ varies with the number of qubits n for these three variants, alongside the same for SK and REM on a hypercube graph, as already shown in figure 7. The variation of P_∞ with the number of qubits n for the five variants is divided into two groups, behaviour like REM and search on the one hand, and behaviour like SK on the other. Removing the correlations from SK by scrambling the energies (sSK) results in behaviour like REM and search. Moreover, removing the correspondence between distance and Hamming weight by using the complete graph instead of the hypercube also changes the SK problem behaviour to be like REM and search. In the opposite direction, inserting pairwise correlations into REM via a Gray code (REMGC) results in problems that are much more like SK than like the REM problems on a hypercube graph.

From this, we infer that the problem structure – in this case the correlations in SK – needs a compatible driver Hamiltonian – in this case the hypercube – to obtain faster than quantum searching. This type of local structure in the solution space is exploited in many classical algorithms. For example, classical Monte Carlo optimizations that use a single bit flip update rule are naturally using this hypercube structure. Using a complete graph instead would amount to flipping a random number of bits, which is equivalent to guessing at each step.

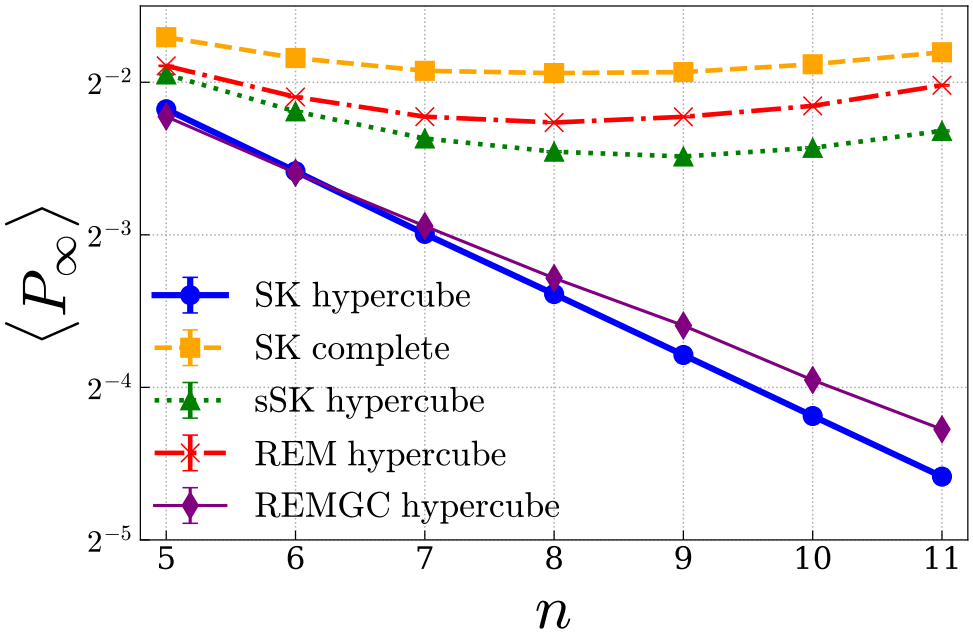

Figure 10. Log-linear plot showing the dependence on number of qubits n of the success-probability P_∞ for SK on hypercube (blue circles, thick solid line), REM on hypercube (red crosses, dash-dotted line), sSK on hypercube (green triangles, dotted line), SK on complete-graph (orange squares, dashed line) and REMGC on hypercube (purple diamonds, thin solid line). The optimal hopping rates $\gamma_{\text{opt}}^{(h)}$ are used in all cases.

6.2. Energy conservation dynamics

Quantum walk time evolution is unitary and there is no time dependence in the Hamiltonian that can lead to energy gain or loss by the system. Therefore, it is important to consider how it can find a lower energy state than it starts in (with respect to $\hat{H}_P$) with any better-than-guessing probability. For the search problem, this happens through an analog of Rabi flopping, cycling between the initial and solution states, but the dominant avoided level crossing structure is not present in the spin glasses to provide this mechanism.

We show here that there is a more general mechanism that relies on starting in the ground state of the quantum walk Hamiltonian $\hat{H}_G$. Let $\langle \hat{O} \rangle_{\psi(t)}$ for operator $\hat{O}$ be defined by $\langle \psi(t)|\hat{O}|\psi(t)\rangle = \langle \hat{O} \rangle_{\psi(t)}$. Then, by the definition of $\hat{H}(\gamma)$ in (8), the energy expectation at time t is

$$\langle \hat{H}(\gamma) \rangle_{\psi(t)} = \langle \hat{H}_G \rangle_{\psi(t)} + \langle \hat{H}_P \rangle_{\psi(t)}. \tag{28}$$

Due to the unitarity of the evolution, this expectation energy will not change over time, giving

$$\langle \hat{H}(\gamma) \rangle_{\psi(t)} = \langle \hat{H}(\gamma) \rangle_{\psi(0)}. \tag{29}$$

which yields

$$\langle \hat{H}_G \rangle_{\psi(t)} - \langle \hat{H}_G \rangle_{\psi(0)} = \langle \hat{H}_P \rangle_{\psi(0)} - \langle \hat{H}_P \rangle_{\psi(t)}. \tag{30}$$

As $|\psi(0)\rangle$ is chosen to be the ground state of $\hat{H}_G$, the LHS must be non-negative. Furthermore, as $|\psi(0)\rangle$ is not an eigenstate of $\hat{H}(\gamma)$, some dynamics are guaranteed to occur and so the LHS must become positive at early times. Therefore, the RHS must also be always non-negative and positive at early times. Thus, taking any final time t_f, we get the inequality

$$\frac{1}{t_f}\int_{t=0}^{t_f} \mathrm{d}t\langle\hat{H}_P\rangle_{\psi(t)} < \langle\hat{H}_P\rangle_{\psi(0)} \tag{31}$$

In summary, performing time evolution under the computational quantum walk Hamiltonian from the initial state $|\psi(0)\rangle$ is guaranteed to lower the energy of the system with respect to $\hat{H}_P$ (the expectation value $\langle\hat{H}_P\rangle_{\psi(t)}$). This implies that the overlap with low energy eigenstates of $\hat{H}_P$ will increase, at least for short times. A measurement in the classical basis is thus more likely to find the ground state, or a state close to it, than a random guess. Starting in a low energy state is thus important for the success of the quantum walk algorithm (we have tested this numerically). It also implies that encoding prior information into the initial state will help, provided this is given as a lower energy state than the uniform superposition state. For many optimization problem applications, it is helpful to find a low energy state, even if it is not actually the true ground state. From this point of view, that quantum walks necessarily lower the expectation energy with respect to the problem Hamiltonian is very appealing as a computational mechanism. This argument by itself does not provide a guaranteed scaling or quantum speed up, but it does explain how the quantum walk dynamics work in this setting, where there is no way to lose (or gain) energy.

To illustrate this in the context of the SK and REM problems of this work, the plots in figure 11 show how the expectation value $\langle\hat{H}_G\rangle_{\psi(t)}$ of the quantum walk Hamiltonian (orange dashed-line) and the expectation value $\langle\hat{H}_P\rangle_{\psi(t)}$ of the problem Hamiltonian (red dotted-line) vary during a quantum walk. We have included the instantaneous success probability $P(t)$ (faint grey) to show that the timescale used is long enough for significant dynamics to take place.

A typical 10-qubit SK example is shown in figure 11(a) and a typical 10-qubit REM example is shown in figure 11(b), both on the hypercube using their respective optimal hopping rates $\gamma^{(h)}_{\mathrm{opt}}$. Also shown in is the ground state eigenvalue $\langle\hat{H}_P\rangle_{E_0^{(P)}}$ of the problem Hamiltonian (red, dash-dotted line) and the ground state eigenvalue $\langle\hat{H}_G\rangle_{\psi(0)}$ of the quantum walk Hamiltonian (green, dashed line). In both SK and REM, the initial evolution takes the state away from the $\hat{H}_G$ ground state, raising the $\hat{H}_G$ expectation value, and thereby lowering the $\hat{H}_P$ expectation value to a point around which it fluctuates for the duration simulated. This clearly shows the energy redistribution mechanism at work, and the short time scale over which it appears.

7. Summary and outlook

In this work we have shown numerically that continuous-time quantum walks are a viable computational method for finding ground states of hard spin glass problems. We have produced strong numerical evidence for a better-than-search polynomial quantum speed up over random guessing, with an average case scaling of $\sim \tilde{O}(N^{0.41})$. Moreoever, this is obtained without the need to set parameters exponentially precisely,

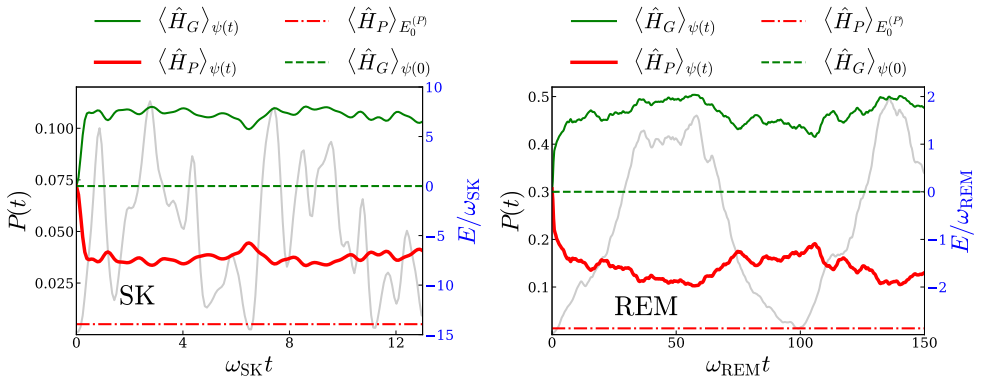

Figure 11. The expectation value $\langle \hat{H}_G \rangle_{\psi(\mathrm{t})}$ of the quantum walk Hamiltonian (green, thin solid line) and the expectation value $\langle \hat{H}_P \rangle_{\psi(\mathrm{t})}$ of the problem Hamiltonian (red, thick solid line) for a typical 10 qubit (a) SK and (b) REM instance. The ground state energy eigenvalues of the quantum walk Hamiltonian (green, dashed line) and problem Hamiltonians (red, dash-dotted line) are also shown. To illustrate that significant dynamics take place over the timescales used, the instantaneous probabilities $P(t)$ are also shown (grey, faint line). The probability values are on the left axes, while energy values are on the right axes.

as is required for quantum walk search algorithms. The hopping rate γ that sets the relative strengths of the quantum walk and problem Hamiltonians can be estimated from the overall energy scales, which are determined by the hardware and encoding of the problem.

To explain why quantum walks are able to do better than quantum searching in this case, we compared variants on the spin glass problems that removed the pairwise correlations, and compared the hypercube graph quantum walk Hamiltonian with the complete graph Hamiltonian. This showed that the combination of pairwise correlations and a matching quantum walk Hamiltonian are required to exploit the correlations. The single spin-flips driven by the transverse field terms $\hat{X}_j$ in the hypercube quantum walk Hamiltonian are the correct operators for the pairwise interaction terms $\hat{Z}_j \hat{Z}_k$ in the spin glass Hamiltonian. A single spin flip on either qubit j or k changes the energy for that term from high to low, or vice versa. Since we can choose how to encode the problems into the Hamiltonians, and there are known methods to convert higher order terms to pairwise terms (Bremner et al., 2002; Dattani, 2019), we can arrange to use this mechanism both for its computational advantages and practicality for hardware implementation.

To explain how quantum walks are able to find low energy states when the closed quantum dynamics have no mechanism for losing energy, we showed how starting in the ground state of the quantum walk part of the Hamiltonian guarantees dynamics that increase the expectation value of the energy with respect to the problem Hamiltonian. This also ensures that prior information can be provided by starting in lower energy states, from which improved solutions can be found.

It is likely that further insights into the computational effectiveness of quantum walks in this Ising Hamiltonian setting can be found by connecting to current

knowledge of spin glass phases in the presence of transverse fields. While the spin glass transition itself is not fully understood, either in the quantum and classical case (see, e.g., Young, 2017; Magalhaes et al., 2017; Thirumalai et al., 1989; Fisher and Huse, 1988, 1987; Larson et al., 2013; Parisi, 1980), the phases of interest for computation are not the spin glass phases themselves, but the phases where transitions between states are still occurring at a rapid enough rate to find solution states. Extremely long equilibration timescales are a defining property of all glass phases, including spin glasses (Cugliandolo, 2002; Bouchaud et al., 1998). Since the equilibration (mixing) times $\tau_{\text{mix}}^{(\epsilon)}$ we find in section 5.3 only scale polynomially with the number of spins, it is likely that the optimal hopping rates $\gamma_{\text{opt}}^{(h)}$ for our quantum walks are not in a finite size precursor to a spin glass phase, but rather in a precursor to a paramagnetic phase, for which equilibration times can be fast. Given that the system should localize more in lower energy states for smaller transverse fields, it is reasonable that our optimal hopping rates $\gamma_{\text{opt}}^{(h)}$ occur near the edge of the precursor to the spin glass phase. Furthermore, the mild scaling of the width $\Delta\gamma_{\text{opt}}^{(h)}$ of the peak around the optimal hopping rate $\gamma_{\text{opt}}^{(h)}$ suggests that the regime where quantum walk performs well may correspond to the second paramagnetic phase observed in Magalhaes et al. (2017).

Performing many repeats of quantum walk computations in early, noisy quantum hardware is a more viable approach than maintaining coherence for sufficiently accurate adiabatic algorithms. Quantum walks may also be simpler to implement since they do not require time dependent controls. This work thus provides a significant advance in the algorithmic understanding of how to exploit quantum walks in practical hardware for optimisation problems.

Acknowledgments

VK and NC funded by UK EPSRC fellowship EP/L022303/1 and NC funded by EPSRC grant EP/S00114X/1. AC gratefully acknowledges funding from EPSRC grant EP/L016524/1 via the CDT in Controlled Quantum Dynamics. We gratefully acknowledge a helpful discussion with Prof. Ifan Hughes.

References

Mohammad H. Amin, Evgeny Andriyash, Jason Rolfe, Bohdan Kulchytskyy, and Roger Melko. Quantum Boltzmann machine. *Phys. Rev. X*, 8:021050, May 2018. doi: 10.1103/PhysRevX.8.021050. URL https://link.aps.org/doi/10.1103/PhysRevX.8.021050.

C. L. Baldwin and C. R. Laumann. Quantum algorithm for energy matching in hard optimization problems. *Phys. Rev. B*, 97:224201, Jun 2018. doi: 10.1103/PhysRevB.97.224201. URL https://link.aps.org/doi/10.1103/PhysRevB.97.224201.

Rene Beier and Berthold Vöcking. Random knapsack in expected polynomial time. *Journal of Computer and System Sciences*, 69(3):306 – 329, 2004. ISSN 0022-0000. doi: https://doi.org/10.1016/j.jcss.2004.04.004. URL http://www.sciencedirect.com/science/article/pii/S0022000004000431. Special Issue on STOC 2003.

C. Bennett, E. Bernstein, G. Brassard, and U. Vazirani. Strengths and Weaknesses of Quantum Computing. *SIAM Journal on Computing*, 26(5):1510–1523, 1997. doi: 10.1137/S0097539796300933. URL https://doi.org/10.1137/S0097539796300933.

Hannes Bernien, Sylvain Schwartz, Alexander Keesling, Harry Levine, Ahmed Omran, Hannes Pichler, Soonwon Choi, Alexander S. Zibrov, Manuel Endres, Markus Greiner, Vladan Vuletić, and Mikhail D. Lukin. Probing many-body dynamics on a 51-atom quantum simulator. *Nature*, 551:579 EP –, 11 2017. URL https://doi.org/10.1038/nature24622.

Zhengbing Bian, Fabian Chudak, William G. Macready, Lane Clark, and Frank Gaitan. Experimental Determination of Ramsey Numbers. *Phys. Rev. Lett.*, 111: 130505, Sep 2013. doi: 10.1103/PhysRevLett.111.130505. URL https://link.aps.org/doi/10.1103/PhysRevLett.111.130505.

Sergio Boixo, Tameem Albash, Federico M. Spedalieri, Nicholas Chancellor, and Daniel A. Lidar. Experimental signature of programmable quantum annealing. *Nature Communications*, 4:2067 EP –, 06 2013. URL https://doi.org/10.1038/ncomms3067.

Jean-Philippe Bouchaud, Leticia F Cugliandolo, Jorge Kurchan, and Marc Mezard. *Out of equilibrium dynamics in spin-glasses and other glassy systems*, pages 161–223. World Scientific, Singapore, 1998. doi: 10.1142/9789812819437_0006. URL https://www.worldscientific.com/doi/abs/10.1142/9789812819437_0006.

Michael J. Bremner, Christopher M. Dawson, Jennifer L. Dodd, Alexei Gilchrist, Aram W. Harrow, Duncan Mortimer, Michael A. Nielsen, and Tobias J. Osborne. Practical Scheme for Quantum Computation with Any Two-Qubit Entangling Gate. *Phys. Rev. Lett.*, 89:247902, Nov 2002. doi: 10.1103/PhysRevLett.89.247902. URL https://link.aps.org/doi/10.1103/PhysRevLett.89.247902.

N. Chancellor, S. Zohren, P. A. Warburton, S. C. Benjamin, and S. Roberts. A Direct Mapping of Max k-SAT and High Order Parity Checks to a Chimera Graph. *Scientific Reports*, 6:37107 EP –, 11 2016. URL https://doi.org/10.1038/srep37107.

Nicholas Chancellor. Modernizing quantum annealing using local searches. *New Journal of Physics*, 19(2):023024, feb 2017. doi: 10.1088/1367-2630/aa59c4. URL https://doi.org/10.1088%2F1367-2630%2Faa59c4.

Nicholas Chancellor, Stefan Zohren, and Paul A. Warburton. Circuit design for multi-body interactions in superconducting quantum annealing systems with applications to a scalable architecture. *npj Quantum Information*, 3(21), 2017. doi: 10.1038/s41534-017-0022-6. URL https://www.nature.com/articles/s41534-017-0022-6.

Andrew M. Childs and Jeffrey Goldstone. Spatial search by quantum walk. *Phys. Rev. A*, 70:022314, Aug 2004. doi: 10.1103/PhysRevA.70.022314. URL https://link.aps.org/doi/10.1103/PhysRevA.70.022314.

Andrew M. Childs, Richard Cleve, Enrico Deotto, Edward Farhi, Sam Gutmann, and Daniel A. Spielman. Exponential Algorithmic Speedup by a Quantum Walk. In *Proceedings of the Thirty-fifth Annual ACM Symposium on Theory of Computing*, STOC '03, pages 59–68, New York, NY, USA, 2003. ACM. ISBN 1-58113-674-9. doi: 10.1145/780542.780552. URL http://doi.acm.org/10.1145/780542.780552.

Vicky Choi. Adiabatic quantum algorithms for the NP-complete Maximum-Weight Independent set, Exact Cover and 3SAT problems. *arXiv preprint arXiv:1004.2226*, 2010. URL https://arxiv.org/abs/1004.2226.

G. E. Coxson, C. R. Hill, and J. C. Russo. Adiabatic quantum computing for finding low-peak-sidelobe codes. In *2014 IEEE High Performance Extreme Computing Conference (HPEC)*, pages 1–6, Sep. 2014. doi: 10.1109/HPEC.2014.7040953. URL https://ieeexplore.ieee.org/abstract/document/7040953.

Leticia F Cugliandolo. Dynamics of glassy systems. *arXiv preprint cond-mat/0210312*, 2002. URL https://arxiv.org/abs/cond-mat/0210312.

D-Wave. D-Wave Systems Inc. website, 1999–. URL http://www.dwavesys.com/. [Online; accessed Wednesday 13th March, 2019].

Nike Dattani. Quadratization in discrete optimization and quantum mechanics. *arXiv preprint arXiv:1901.04405*, 2019. URL http://arxiv.org/abs/1901.04405.

Gemma De las Cuevas and Toby S. Cubitt. Simple universal models capture all classical spin physics. *Science*, 351(6278):1180–1183, 2016. ISSN 0036-8075. doi: 10.1126/science.aab3326. URL http://science.sciencemag.org/content/351/6278/1180.

B. Derrida. Random-Energy Model: Limit of a Family of Disordered Models. *Phys. Rev. Lett.*, 45:79–82, Jul 1980. doi: 10.1103/PhysRevLett.45.79. URL https://link.aps.org/doi/10.1103/PhysRevLett.45.79.

Ben Dodds, Viv Kendon, Charles S Adams, and Nicholas Chancellor. Practical designs for permutation symmetric problem Hamiltonians on hypercubes. *arXiv preprint arXiv:1812.07885*, 2018. URL https://arxiv.org/abs/1812.07885.

Edward Farhi, Jeffrey Goldstone, Sam Gutmann, and Michael Sipser. Quantum computation by adiabatic evolution. *arXiv preprint quant-ph/0001106*, 2000. URL https://arxiv.org/abs/quant-ph/0001106.

Edward Farhi, Jeffrey Goldstone, Sam Gutmann, Joshua Lapan, Andrew Lundgren, and Daniel Preda. A Quantum Adiabatic Evolution Algorithm Applied to Random Instances of an NP-Complete Problem. *Science*, 292(5516):472–475, 2001. ISSN 0036-8075. doi: 10.1126/science.1057726. URL http://science.sciencemag.org/content/292/5516/472.

Edward Farhi, Jeffrey Goldstone, Sam Gutmann, and Daniel Nagaj. How to make the quantum adiabatic algorithm fail. *International Journal of Quantum Information*, 06(03):503–516, 2008. doi: 10.1142/S021974990800358X. URL https://doi.org/10.1142/S021974990800358X.

Edward Farhi, Jeffrey Goldstone, David Gosset, Sam Gutmann, and Peter Shor. Unstructured randomness, small gaps and localization. *arXiv preprint arXiv:1010.0009*, 2010. URL https://arxiv.org/abs/1010.0009.

Edward Farhi, Jeffrey Goldstone, and Sam Gutmann. A quantum approximate optimization algorithm. *arXiv preprint arXiv:1411.4028*, 2014a. URL https://arxiv.org/abs/1411.4028.

Edward Farhi, Jeffrey Goldstone, and Sam Gutmann. A quantum approximate optimization algorithm applied to a bounded occurrence constraint problem. *arXiv preprint arXiv:1412.6062*, 2014b. URL https://arxiv.org/abs/1412.6062.

Sheng Feng, Ye Fang, Ka-Ming Tam, Zhifeng Yun, J Ramanujam, Juana Moreno, and Mark Jarrell. Three Dimensional Edwards-Anderson Spin Glass Model in an

External Field. *arXiv preprint arXiv:1403.4560*, 2014. URL https://arxiv.org/abs/1403.4560.

A.B. Finnila, M.A. Gomez, C. Sebenik, C. Stenson, and J.D. Doll. Quantum annealing: A new method for minimizing multidimensional functions. *Chemical Physics Letters*, 219(5):343 – 348, 1994. ISSN 0009-2614. doi: https://doi.org/10.1016/0009-2614(94)00117-0. URL http://www.sciencedirect.com/science/article/pii/0009261494001170.

D S Fisher and D A Huse. Absence of many states in realistic spin glasses. *Journal of Physics A: Mathematical and General*, 20(15):L1005–L1010, oct 1987. doi: 10.1088/0305-4470/20/15/013. URL https://doi.org/10.1088%2F0305-4470%2F20%2F15%2F013.

Daniel S. Fisher and David A. Huse. Equilibrium behavior of the spin-glass ordered phase. *Phys. Rev. B*, 38:386–411, Jul 1988. doi: 10.1103/PhysRevB.38.386. URL https://link.aps.org/doi/10.1103/PhysRevB.38.386.

Lov K. Grover. A Fast Quantum Mechanical Algorithm for Database Search. In *Proceedings of the Twenty-eighth Annual ACM Symposium on Theory of Computing*, STOC '96, pages 212–219, New York, NY, USA, 1996. ACM. ISBN 0-89791-785-5. doi: 10.1145/237814.237866. URL http://doi.acm.org/10.1145/237814.237866.

Stuart Hadfield, Zhihui Wang, Bryan OGorman, Eleanor G. Rieffel, Davide Venturelli, and Rupak Biswas. From the Quantum Approximate Optimization Algorithm to a Quantum Alternating Operator Ansatz. *Algorithms*, 12(2), 2019. ISSN 1999-4893. doi: 10.3390/a12020034. URL http://www.mdpi.com/1999-4893/12/2/34.

John D Hunter. Matplotlib: A 2Dgraphics environment. *Computing in science & engineering*, 9(3):90, 2007.

Takahiro Inagaki, Yoshitaka Haribara, Koji Igarashi, Tomohiro Sonobe, Shuhei Tamate, Toshimori Honjo, Alireza Marandi, Peter L. McMahon, Takeshi Umeki, Koji Enbutsu, Osamu Tadanaga, Hirokazu Takenouchi, Kazuyuki Aihara, Ken-ichi Kawarabayashi, Kyo Inoue, Shoko Utsunomiya, and Hiroki Takesue. A coherent Ising machine for 2000-node optimization problems. *Science*, 354(6312):603–606, 2016. ISSN 0036-8075. URL http://science.sciencemag.org/content/354/6312/603.

M. W. Johnson, M. H. S. Amin, S. Gildert, T. Lanting, F. Hamze, N. Dickson, R. Harris, A. J. Berkley, J. Johansson, P. Bunyk, E. M. Chapple, C. Enderud, J. P. Hilton, K. Karimi, E. Ladizinsky, N. Ladizinsky, T. Oh, I. Perminov, C. Rich, M. C. Thom, E. Tolkacheva, C. J. S. Truncik, S. Uchaikin, J. Wang, B. Wilson, and G. Rose. Quantum annealing with manufactured spins. *Nature*, 473:194 EP –, 05 2011. URL https://doi.org/10.1038/nature10012.

Eric Jones, Travis Oliphant, Pearu Peterson, et al. SciPy: Open source scientific tools for Python, 2001–. URL http://www.scipy.org/. [Online; accessed Wednesday 13th March, 2019].

Tadashi Kadowaki and Hidetoshi Nishimori. Quantum annealing in the transverse Ising model. *Phys. Rev. E*, 58:5355–5363, Nov 1998. doi: 10.1103/PhysRevE.58.5355. URL https://link.aps.org/doi/10.1103/PhysRevE.58.5355.

Helmut G. Katzgraber, Firas Hamze, and Ruben S. Andrist. Glassy Chimeras Could Be Blind to Quantum Speedup: Designing Better Benchmarks for Quantum

Annealing Machines. *Phys. Rev. X*, 4:021008, Apr 2014. doi: 10.1103/PhysRevX.4.021008. URL https://link.aps.org/doi/10.1103/PhysRevX.4.021008.

Thomas Kluyver, Benjamin Ragan-Kelley, Fernando Pérez, Brian Granger, Matthias Bussonnier, Jonathan Frederic, Kyle Kelley, Jessica Hamrick, Jason Grout, Sylvain Corlay, Paul Ivanov, Damián Avila, Safia Abdalla, and Carol Willing. Jupyter Notebooks – a publishing format for reproducible computational workflows. In F. Loizides and B. Schmidt, editors, *Positioning and Power in Academic Publishing: Players, Agents and Agendas*, pages 87 – 90. IOS Press, 2016.

Michael Krivelevich and Dan Vilenchik. Solving Random Satisfiable 3CNF Formulas in Expected Polynomial Time. In *Proceedings of the Seventeenth Annual ACM-SIAM Symposium on Discrete Algorithm*, SODA '06, pages 454–463, Philadelphia, PA, USA, 2006. Society for Industrial and Applied Mathematics. ISBN 0-89871-605-5. URL http://dl.acm.org/citation.cfm?id=1109557.1109608.

Derek Larson, Helmut G. Katzgraber, M. A. Moore, and A. P. Young. Spin glasses in a field: Three and four dimensions as seen from one space dimension. *Phys. Rev. B*, 87:024414, Jan 2013. doi: 10.1103/PhysRevB.87.024414. URL https://link.aps.org/doi/10.1103/PhysRevB.87.024414.

Zhaokai Li, Nikesh S Dattani, Xi Chen, Xiaomei Liu, Hengyan Wang, Richard Tanburn, Hongwei Chen, Xinhua Peng, and Jiangfeng Du. High-fidelity adiabatic quantum computation using the intrinsic Hamiltonian of a spin system: Application to the experimental factorization of 291311. *arXiv preprint arXiv:1706.08061*, 2017. URL https://arxiv.org/abs/1706.08061.

Neil B Lovett, Matthew Everitt, Robert M Heath, and Viv Kendon. The quantum walk search algorithm: factors affecting efficiency. *Mathematical Structures in Computer Science*, 29(3):389429, 2019. doi: 10.1017/S0960129518000051. URL https://doi.org/10.1017/S0960129518000051.

Andrew Lucas. Ising formulations of many NP problems. *Frontiers in Physics*, 2: 5, 2014. ISSN 2296-424X. doi: 10.3389/fphy.2014.00005. URL https://www.frontiersin.org/article/10.3389/fphy.2014.00005.

S. G. Magalhaes, C. V. Morais, F. M. Zimmer, M. J. Lazo, and F. D. Nobre. Nonlinear susceptibility of a quantum spin glass under uniform transverse and random longitudinal magnetic fields. *Phys. Rev. B*, 95:064201, Feb 2017. doi: 10.1103/PhysRevB.95.064201. URL https://link.aps.org/doi/10.1103/PhysRevB.95.064201.

S. Marsh and J. B. Wang. A quantum walk-assisted approximate algorithm for bounded NP optimisation problems. *Quantum Information Processing*, 18(3): 61, Jan 2019. ISSN 1573-1332. doi: 10.1007/s11128-019-2171-3. URL https://doi.org/10.1007/s11128-019-2171-3.

Jeffrey Marshall, Davide Venturelli, Itay Hen, and Eleanor G Rieffel. The power of pausing: advancing understanding of thermalization in experimental quantum annealers. *arXiv preprint arXiv:1810.05881*, 2018. URL https://arxiv.org/abs/1810.05881.

Michael Marzec. *Portfolio Optimization: Applications in Quantum Computing*, chapter 4, pages 73–106. John Wiley & Sons, Ltd, 2016. ISBN 9781118593486. doi: 10.1002/9781118593486.ch4. URL https://onlinelibrary.wiley.com/doi/abs/10.1002/9781118593486.ch4.

Wes McKinney et al. Data structures for statistical computing in python. In *Proceedings of the 9th Python in Science Conference*, volume 445, pages 51–56. Austin, TX, 2010.

Peter L. McMahon, Alireza Marandi, Yoshitaka Haribara, Ryan Hamerly, Carsten Langrock, Shuhei Tamate, Takahiro Inagaki, Hiroki Takesue, Shoko Utsunomiya, Kazuyuki Aihara, Robert L. Byer, M. M. Fejer, Hideo Mabuchi, and Yoshihisa Yamamoto. A fully programmable 100-spin coherent Ising machine with all-to-all connections. *Science*, 354(6312):614–617, 2016. ISSN 0036-8075. doi: 10.1126/science.aah5178. URL http://science.sciencemag.org/content/354/6312/614.

James G. Morley, Nicholas Chancellor, Sougato Bose, and Viv Kendon. Quantum search with hybrid adiabatic–quantum-walk algorithms and realistic noise. *Phys. Rev. A*, 99:022339, Feb 2019. doi: 10.1103/PhysRevA.99.022339. URL https://link.aps.org/doi/10.1103/PhysRevA.99.022339.

Travis E Oliphant. *A guide to NumPy*, volume 1. Trelgol Publishing USA, 2006.

G Parisi. The order parameter for spin glasses: a function on the interval 0-1. *Journal of Physics A: Mathematical and General*, 13(3):1101–1112, mar 1980. doi: 10.1088/0305-4470/13/3/042. URL https://doi.org/10.1088%2F0305-4470%2F13%2F3%2F042.

G Passarelli, V Cataudella, and P Lucignano. Improving the quantum annealing of the ferromagnetic p-spin model through pausing. *arXiv preprint arXiv:1902.06788*, 2019. URL https://arxiv.org/abs/1902.06788.

Alejandro Perdomo-Ortiz, Salvador E. Venegas-Andraca, and Alán Aspuru-Guzik. A study of heuristic guesses for adiabatic quantum computation. *Quantum Information Processing*, 10(1):33–52, Feb 2011. ISSN 1573-1332. doi: 10.1007/s11128-010-0168-z. URL https://doi.org/10.1007/s11128-010-0168-z.

Alejandro Perdomo-Ortiz, Neil Dickson, Marshall Drew-Brook, Geordie Rose, and Alán Aspuru-Guzik. Finding low-energy conformations of lattice protein models by quantum annealing. *Scientific Reports*, 2:571 EP –, 08 2012. URL https://doi.org/10.1038/srep00571.

F. Perez and B. E. Granger. IPython: A System for Interactive Scientific Computing. *Computing in Science Engineering*, 9(3):21–29, May 2007. ISSN 1521-9615. doi: 10.1109/MCSE.2007.53.

Neil Shenvi, Julia Kempe, and K. Birgitta Whaley. Quantum random-walk search algorithm. *Phys. Rev. A*, 67:052307, May 2003. doi: 10.1103/PhysRevA.67.052307. URL https://link.aps.org/doi/10.1103/PhysRevA.67.052307.

David Sherrington and Scott Kirkpatrick. Solvable Model of a Spin-Glass. *Phys. Rev. Lett.*, 35:1792–1796, Dec 1975. doi: 10.1103/PhysRevLett.35.1792. URL https://link.aps.org/doi/10.1103/PhysRevLett.35.1792.

D Thirumalai, Qiang Li, and T R Kirkpatrick. Infinite-range Ising spin glass in a transverse field. *Journal of Physics A: Mathematical and General*, 22(16):3339–3349, aug 1989. doi: 10.1088/0305-4470/22/16/023. URL https://doi.org/10.1088%2F0305-4470%2F22%2F16%2F023.

Guido Van Rossum and Fred L Drake. *Python language reference manual*. Network Theory United Kingdom, 2003.

A. P. Young. Stability of the quantum Sherrington-Kirkpatrick spin glass model. *Phys. Rev. E*, 96:032112, Sep 2017. doi: 10.1103/PhysRevE.96.032112. URL https://link.aps.org/doi/10.1103/PhysRevE.96.032112.

A. P. Young and Helmut G. Katzgraber. Absence of an Almeida-Thouless Line in Three-Dimensional Spin Glasses. *Phys. Rev. Lett.*, 93:207203, Nov 2004. doi: 10.1103/PhysRevLett.93.207203. URL https://link.aps.org/doi/10.1103/PhysRevLett.93.207203.